Comparison of existing electrode designs for preferential activation of cutaneous nociceptors

Poulsen, Aida Hejlskov; Tigerholm, Jenny; Meijs, Suzan; Andersen, Ole Kaeseler; Mørch, Carsten Dahl

Published in:
Journal of Neural Engineering

DOI (link to publication from Publisher):
10.1088/1741-2552/ab85b1

Publication date:
2020

Document Version
Accepted author manuscript, peer reviewed version

Journal of Neural Engineering

Comparison of existing electrode designs for preferential activation of cutaneous nociceptors

To cite this article before publication: Aida Hejlskov Poulsen *et al* 2020 *J. Neural Eng.* in press https://doi.org/10.1088/1741-2552/ab85b1

Comparison of existing electrode designs for preferential activation of cutaneous nociceptors

Authors: Aida Hejlskov Poulsen*, Jenny Tigerholm*, Suzan Meijs*, Ole Kæseler Andersen*, Carsten Dahl Mørch*

*Center for Neuroplasticity and Pain (CNAP), Department of Health Science and Technology, Aalborg University, Aalborg, Denmark

Abstract

Objective. Over the recent years, several small area electrodes have been introduced as tools for preferential stimulation of small cutaneous nerve fibers. However, the performance of the electrodes is highly debated and have not previously been systematically compared. The electrodes have been developed empirically and little is known about the electrical potential they produce in the skin, and how this influences the nerve fiber activation. The objective of the present study was to develop and validate a computational model to compare the preferential stimulation of small fibers for electrodes of different designs.

Approach. A finite element model of the skin was developed and coupled with an Aβ-fiber and an Aδ-fiber multi-compartmental nerve fiber model, to describe the current spread and consequent nerve fiber activation produced by five different surface electrodes; intra-epidermal, planar concentric, pin, planar array, and patch. The model was validated through experimental assessments of the strength-duration relationship, impedance and reaction times.

Main results. The computational model predicted the intra-epidermal electrode to be the most preferential for small fiber activation. The intra-epidermal electrode was however also found to be the most sensitive to positioning relative to nerve fiber location, which may limit the practical use of the electrode.

Significance. The present study highlights the influence of different electrode design features on the current spread and resulting activation of cutaneous nerve fibers. Additionally, the computational model may be used for the optimization of electrode design towards even better preferential stimulation of small fibers.

1. Introduction

Probing the pain system using a nociceptive selective stimulus, is an important instrument for assessing the integrity and functional status of the pain pathways [1], [2] as well as for pain control and modification [3]–[5]. Additionally, nociceptive selective stimulation is essential for electrophysiological studies to understand the mechanism of pain processing and the pathophysiology of different pain syndromes. Selectively activating the nociceptive system is however a challenging task, that demands specialized equipment. Often, laser stimulation is used to selectively activate small nociceptive fibers, i.e. Aδ- and C-fibers without concomitant activation of large non-nociceptive Aβ-fibers [6]. However, lasers are very expensive and limited in their use in relation to possible application areas, different pulse shapes, and the risk of skin lesion [6], [7]. Due to these limitations, specialized electrodes have been suggested as an alternative tool for activation of small nociceptive nerve fibers [3], [8]–[11]. Conventional transcutaneous electrical stimulation using regular patch electrodes activates large fibers at a lower intensity than small fibers. However, it is possible to change the order of recruitment, by generating a high current density in the superficial layers of the skin, where the small fibers terminate, and limit the current spread to deeper tissues, where the large fibers terminate [9], [12], [13]. This can be achieved by the use of small area or intra-epidermal cathodes and concentric electrode configurations [3], [8]–[10], [13]. These electrodes evoke a pinprick sensation [3], [8]–[10], delayed cortical potentials [7], [14]–[17] of bilateral origin [18], and delayed reaction times [14], [19], all indicating preferential activation of small nociceptive fibers. However, concomitant activation of large fibers cannot be excluded, and becomes especially pronounced when the intensity of the stimulation exceeds two times the perception threshold [7], [16].

Existing electrodes, designed for small fiber stimulation, have not been directly compared and it is unclear if and how different electrode designs influence the ability to preferentially activate small fibers. The electrodes have all been developed empirically and only a few design features such as cathode diameter [13], length of protruding elements and anode surface area [20] have been evaluated through computational modeling. Computational modeling enables comparison of electrode designs, as it is possible to describe the electrical potential generated in the skin and the resulting nerve fiber activation, in relation to specific electrode designs.

The aim of the present work was therefore to compare the nerve fiber activation between available electrode designs. Therefore a computational model was constructed and validated. The model was

composed of a finite element model of the skin at the volar forearm, to simulate the generated electrical potential in the skin, and two multi-compartmental models of an Aβ- and Aδ-fiber with a wide range of voltage-gated ion channels [21] to quantify the resulting excitation of cutaneous nerve fibers. The model was validated through experimental assessments of electrode impedances, perception thresholds and reaction times.

2. Methods

Five surface electrodes (four designed for preferential small fiber activation and a regular patch electrode) were modeled in a two-step hybrid model fashion, to investigate the influence of electrode design on the electrical potential produced in the skin and the resulting activation of cutaneous nerve fibers (figure 1). The first model step was a finite element model (COMSOL Multiphysics 5.3, Stockholm, Sweden), which described the electrical potential generated in the skin. The second step of the model contained two multi-compartmental axon models (NEURON, Yale, USA [22]) of an Aδ- and an Aβ-fiber axon, to describe the nerve fiber activation [21].

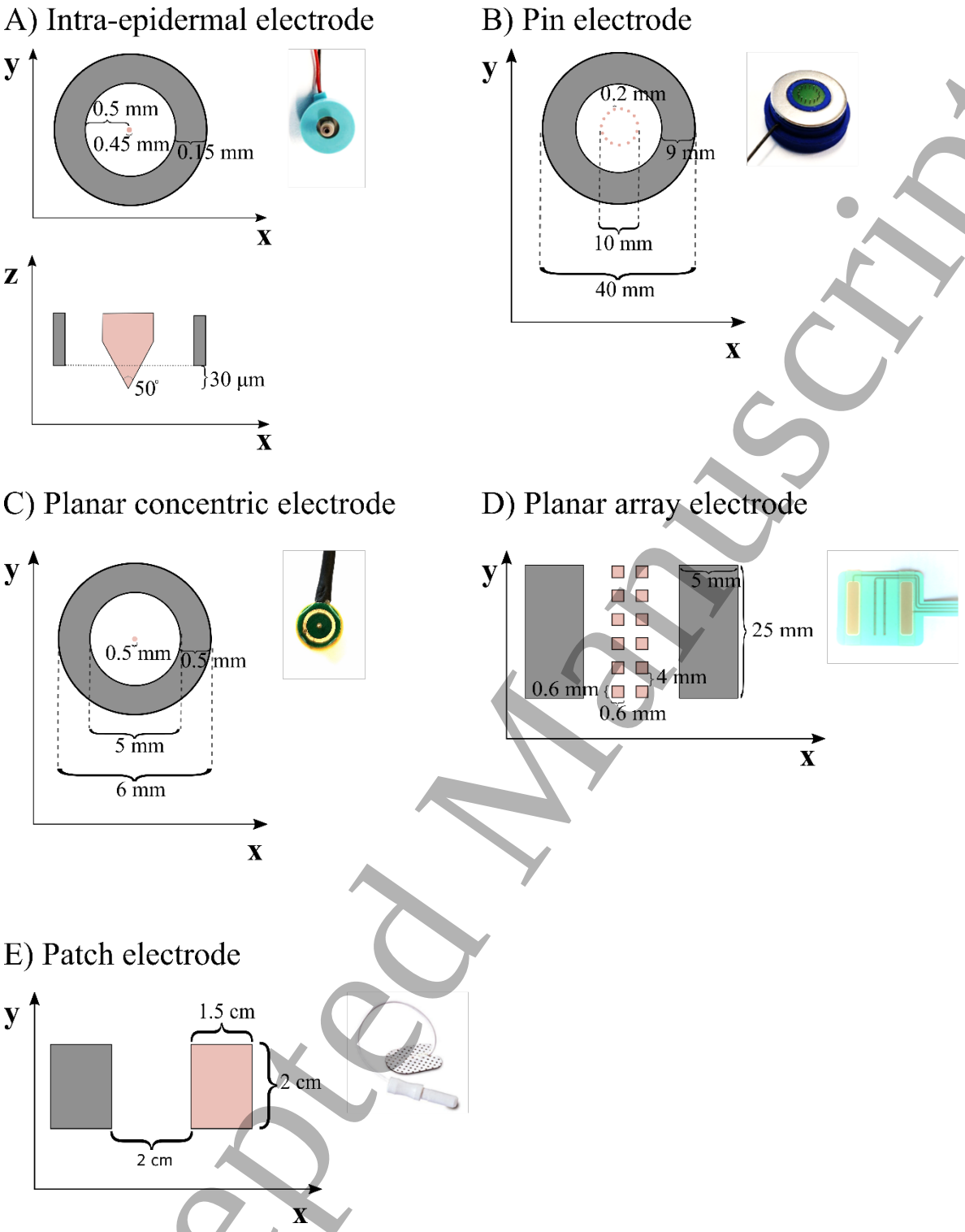

Figure 1: Spatial dimensions of the modeled electrodes. Not drawn to scale. Red areas indicate the cathode(s), while the dark grey areas indicate the anode(s). A) The intra-epidermal electrode has a concentric design with a protruding stainless steel needle penetrating the stratum corneum [8]. *B) The pin electrode has 15 interconnected pin cathodes and a concentric anode, all made of stainless steel* [23]. *C) The planar concentric electrode has a small metal cathode in the center and a concentric anode* [9]. *D) The planar array electrode has 12 interconnected square cathodes and two rectangular anodes, the electrode is printed with conocting paste on a flexible PET base* [24]. *E) The regular Ag-AgCl patch electrode consists of two large surface area rectangles (Ambu® neuroline 700).*

2.1 Finite element model of the skin

The extracellular potential was calculated through either a 2D-axisymmetrical model (for the planar concentric and intra-epidermal electrode) or a 3D model (for the pin, planar array, and patch electrodes) of the skin at the volar forearm. The models were further developed from the finite element model presented by Mørch et al [13]. The skin model consisted of the four horizontal, homogeneous skin layers; stratum corneum, epidermis, dermis, and hypodermis (see figure 2). The thickness and electrical properties of the four skin layers were adopted from literature. The values from Yamamoto and Yamamoto [25] and Tavernier et al [26], were interpolated from the presented graphs and fitted to a power function of the frequency (f). The electrical properties used in the finite element models are presented in table 1.

The electrode skin interface was included in the models as a thin 10 µm layer between the electrode and the skin, and the conductivity and permittivity of the interface was deduced by the resistance and capacitance values presented by Chi et al [27], for all electrodes. As the regular patch electrode was covered by a conductive gel, an additional rectangular layer of conductive hydrogel was modeled under this electrode (see electrical properties in table 1). Otherwise, electrode materials were not included in the models. According to recommendations by Pelot et al [28] a normal current density and ground condition was employed to the model to achieve a high accuracy and computational efficiency. A total current of 1 mA and -1 mA was evenly distributed on the surface of the interface or hydrogel layer of cathode and anode, respectively. The ground condition was applied to the bottom of the hypodermal layer (see supplementary figures S15-18 for investigations of the ground influence on the electrical potential). All other external boundaries were considered electrically insulated, while current continuity conditions were applied to the inner boundaries. A mesh of free triangular elements was generated for the axisymmetric models, while a swept mesh of hexahedron elements, based on free triangular elements, was generated for the 3D models. The mesh density was highest at the electrode edges, where the current density was expected to be highest. To ensure adequate mesh density and model side length, convergence studies were performed. The mesh density or model size was gradually increased until the change in the electrical potential, from the previous increment, became less than 0.1 mV. Final model side length, maximum and minimum element sizes, and

average element quality are listed in table 2 (See supplementary figures S12-S16 for mesh illustrations).

Table 1: Thickness and electrical conductivity and permittivity of different material layers included in the model. For most of the properties, a frequency (f) dependency was implemented. Functions for the stratum corneum were derived from fitting data of the figures presented by [29]. *Functions for the relative permittivity of the epidermis and dermis were derived from fitting the data of the figures presented by* [26]. *For the skin-electrode interface the resistance and capacitance values from* [27] *was used together with the thickness of the interface layer, the area of the electrode, and the permittivity of vacuum (ε_0) to calculate the corresponding conductivity and permittivity for the interface layer.*

Skin model layer	**Thickness (µm)**	**Electrical conductivity (S/m)**	**Relative electrical permittivity**
Stratum corneum	20 [30]–[35]	$\frac{1}{1.339*10^5*f^{-0.1099}*(-3.65)*10\text{^}4}$ [25]	$1.44*10^4*f^{-0.459}+1{,}285$ [25]
Epidermis	82 [31], [33], [34]	Horizontal: 0.95 [26] Vertical: 0.15 [26]	$-1.332*f^{-1.212}+3.731*10^5$ [26] $6.32*10^6*f^{-0.562}-1.196*10^4$ [26]
Dermis	1300[36]	Horizontal: 2.57 [26] Vertical: 1.62 [26]	$5.394*10^8*f^{-1.012}+2.301*10\text{^}5$ [26] $3.255*10^9*f^{-1.25}-8{,}433$ [26]
Hypodermis	5000	$2.3*10^{-2}$ [37], [38]	$1*10^3$ [37], [38]
Skin-electrode interface	10	Wet: [27] $\frac{interfaceThickness}{350^3*ElectrodeArea}$ Dry: [27] $\frac{interfaceThickness}{1.3^6*ElectrodeArea}$	Wet: [27] $\frac{25^{-9}*interfaceThickness}{\varepsilon_0*ElectrodeArea}$ Dry: [27] $\frac{12^{-9}*interfaceThickness}{\varepsilon_0*ElectrodeArea}$
Hydrogel	1000	0.0149	5000

Table 2: Model size and mesh element restrictions and average quality for each electrode model. The skin model was a square model and the model size refers to the length of the sides of the square. The mesh consisted of free triangular and swept hexahedron elements.

Electrode	Model Size (cm)	Maximum element size (m)	Minimum element size (m)	Average mesh quality (COMSOL skewness measure)
Intra-epidermal [8]	11	0.0037	2.1e-5	0.9019
Pin [23]	10	0.0037	2.1e-5	0.8771
Planar concentric [9]	5	0.0015	1e-6	0.9007
Planar array [24]	7	0.0026	1.1e-5	0.8943
Patch (Ambu® neuroline 700)	15	0.0015	1e-6	0.9150

To investigate the complex impedance response as a function of frequencies for all electrodes, a frequency domain study was conducted for each electrode model. In the frequency domain study, the time-harmonic equation of continuity was used for calculation of the electric potential:

$$-\nabla \cdot \left((\sigma + j\omega\varepsilon_0\varepsilon_r)\nabla V_{FE} - \boldsymbol{J}_e\right) = 0$$

Where σ is the conductivity, ε_0 is the permittivity of vacuum and ε_r is the relative permittivity. V_{FE} is the electrical potential calculated by the finite element model and $\boldsymbol{J}_e$ the external current density that was applied only to the areas of the electrodes. The study was conducted for frequencies between 10 Hz and 100 kHz with ten frequencies per decade.

The frequency dependencies of the tissues were important to capture the impedance response of the electrodes, however, preliminary investigations of the time-dependent solution revealed a limited effect of the tissue permittivity and frequency dependencies over the time course of the square pulses used for simulations (0.1, 0.5, 1, and 10 ms) (see supplementary material figure S1). Consequently, it was considered a reasonable approximation to omit the effect of permittivity and use the steady-state solution to investigate the distribution of the electrical potential in the different skin layers, and to extract the extracellular potential at the nerve fiber location. All other simulations than the one for

the impedance were thus computed from the steady-state solutions calculated by the quasi-static form of the continuity equation described by Laplace's equation:

$$-\nabla \cdot (\sigma \nabla V_{FE} - \boldsymbol{J}_e) = 0$$

2.2 Axon models

The nerve fiber activation resulting from changes in the extracellular potential was simulated through an Aδ-fiber model and an Aβ-fiber model developed by Tigerholm et al [21]. The models will be briefly described here, however for a more detailed description the reader is referred to Tigerholm et al [21]. The nerve fiber models were implemented in the NEURON environment, as representations of the average of the nerve fiber populations. The Aβ-fiber model had a diameter of 9 µm, was 4.994 cm long and consisted of 27,120 compartments (1.8 compartments/µm). The model ran horizontally in the hypodermal layer prior to making a 45 degrees angled branch that ascended in a straight line and terminated in the dermis (see figure 2). The Aδ-fiber model followed a similar path, however terminating as a free unmyelinated nerve ending in the epidermis after losing its myelin at the dermal-epidermal junction [39]. Furthermore, two small side branches, branched out in the epidermis with an angle of 90 degrees from the main branch and equally distanced to produce a nerve fiber density of 17 free nerve endings per millimeter [40]. A total of 26,088 compartments (2 compartements/µm) made up the Aδ-fiber model with a total length of 5.472 cm and a diameter of 3.5 µm. The ion channels of the nerve fiber models were implemented as Hodgkin-Huxley-type ion channels and included: Nav1.6, Nav1.7, Nav1.8, Nav1.9, K_{dr}, K_M, K_A, and the hyperpolarization-activated and cyclic nucleotide-gated (HCN) channels.

The electrical potential calculated by the finite element model was used as the extracellular potential input to the axon models, by interpolating the potential onto the locations corresponding to the nerve fiber positions. The extracellular potential was multiplied by a step-function corresponding to the stimulation pulse durations and linearly increased to find the nerve fiber activation threshold, which was defined as the stimulation current needed to generate an action potential that propagated to the end of the axon model, and was determined by solving the model using the variable time step method. The action potentials were initiated at the tip of the nerve fiber models for all other electrodes than the patch, which activated the Aδ-fiber model at the first node of ranvier.

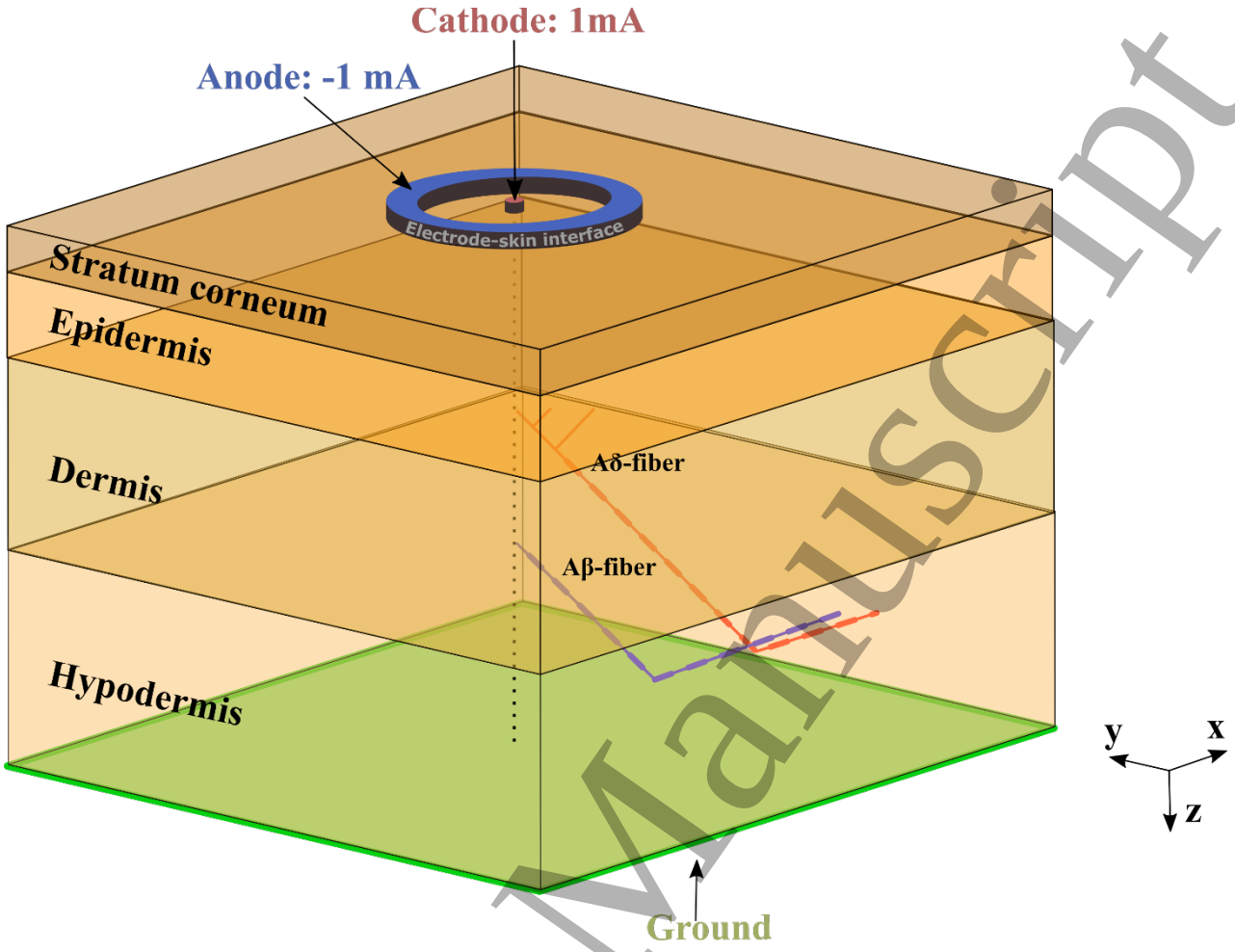

Figure 2: Example of the combined skin and nerve fiber model for the concentric electrode, not drawn to scale. The skin model consisted of four layers; stratum corneum, epidermis, dermis, and hypodermis. The bottom of the hypodermis was grounded. The electrode model consisted of the cathode and anode and an additional electrode-skin interface layer. The nerve fiber models were located directly under the cathode and followed similar paths, except the Aβ-fiber model terminated in the middle of the dermis and the Aδ-fiber model terminated in the middle of the epidermis. The Aδ-fiber model lost its myelin at the epidermal-dermal junction.

The area of selectivity was defined as a 2D area in the x-y plane, for which the activation threshold of the Aδ-fiber model is lower than that of the Aβ-fiber model. When the nerve fiber models were located directly under the cathode, for which location the activation threshold was at a minimum, the activation threshold for the Aδ-fiber model was lower than for the Aβ-fiber model, for all other electrodes than the regular patch. Therefore, the area of selectivity was only investigated for the electrodes developed for small fiber activation. Simulations were performed with 0.1 and 10 ms rectangular pulses in both the x and y direction. The Aδ-fiber model was initially located directly under the center of the cathode. If the activation threshold was lower than that of the Aβ-fiber model, the distance from the Aδ-fiber model to the center of the cathode was increased in either the x or y

direction. When the Aδ-fiber model activation threshold became higher than that of the Aβ-fiber model, the distance was decreased. The calculations were terminated when the difference in activation threshold between the Aβ-fiber model and the Aδ-fiber model was less than 10 μA, corresponding to the accuracy of the nerve fiber model. The area of selectivity was evaluated at three different termination depths of the Aδ-fiber model with the nerve fiber ending positioned at z = 21, 61, or 101 μm, all within the epidermis.

Furthermore, the strength-duration relationship was evaluated for rectangular pulses of 0.1, 0.5, 1, and 10 ms duration, at 12 random spatial locations of the nerve fiber models. The locations of the Aδ-fiber model were restricted to the calculated area of selectivity, as it was assumed that mainly the fibers within this area are activated with the small fiber preferential electrodes and thus are the main contributors to the perception threshold. The locations for the Aβ-fiber model were randomly chosen in a horizontal radius of 600 μm from the center of the cathode and at depths between 702-792 μm corresponding to the middle of the dermis ± 40 μm. The number of included locations were determined by including one location at the time and evaluating the change in the average activation threshold of all included locations. No more locations were added when the change in the average was less than 1 μA.

2.3 Experimental validation

Fifteen healthy volunteers (aged 20-39) participated in the study. All participants gave written, informed consent according to the Declaration of Helsinki, prior to participation. The study was approved by the local ethics committee (ref. no N-20180050).

Measurements of impedances, strength-duration curves, and reaction times were performed for all five modeled electrodes. The subject was seated in the laboratory 10 minutes prior to the first measurement in order to adjust to the environment. The skin was cleaned with alcohol wipes prior to electrode placement. The electrodes for small fiber stimulation were placed on the volar forearm, with the center of the electrode 5 cm distal to the elbow joint. For the regular patch electrode, the

center of the cathode was placed 5 cm distal to the elbow joint and the anode was placed 2 cm distal to the cathode.

Impedances were acquired with the frequency response analyzer Solartron 1260 and the Solartron 1294 impedance interface (Ametek Scientific instruments, Farnborough, USA), in a two-point setup. The impedance was measured as the ratio of the measured voltage across the electrodes when applying a low amplitude (30 μA) constant sine wave stimuli (50 cycles), in the frequency range of 10 Hz to 100 kHz, with 10 measurement points per decade.

The strength-duration curve can be used to describe the excitability of the activated nerve fibers [41]–[43]. The rheobase, defined as the stimulus intensity required to reach nerve activation for an infinitely long pulse, and the chronaxie, defined as the pulse duration corresponding to an intensity two times the rheobase, differ between nerve fiber types [41], [44]. The strength-duration curves were obtained through perception threshold determination of four rectangular pulses, with durations of 0.1, 0.5, 1, and 10 ms [43]. The pulse durations and the order of the electrodes were randomized between subjects. Rheobase and chronaxie values were subsequently estimated by Weiss law [45].

The perception threshold was determined through a modified method of limits, where the limits were defined as three consecutive perceived or not perceived stimuli in four ascending and four descending measures, respectively [43], [44]. The inter-stimulus interval was randomized between 2.5 and 3.5 seconds. The stimulus intensity started at 0.1 mA and increased with 20 % until the subject by the click of a button had indicated three perceived stimuli at the same intensity. Then the intensity decreased with 20 % until the subject had not indicated perception for three consecutive stimulations at the same intensity. For the following three sequences the intensity was increased and decreased with 12%, 8%, and 5% (see figure 3). The final threshold was calculated as a weighted average of ascending and descending limits with weights corresponding to the inverse of the corresponding step size.

Reaction times were recorded during threshold determination as an indirect measure of nerve conduction, by instructing the subject to push a button as fast as possible whenever a stimulus was perceived. The 4x3 reaction time recordings, for consecutive perceived stimuli at the ascending limits, for each pulse and subject were included for analysis (see red circles in figure 3). Reaction times below 100 ms were discarded as results of anticipation or fast guessing. Additionally, reaction times

above 1,500 ms were considered to be related to undetected stimuli or poor attention and were discarded from further analysis.

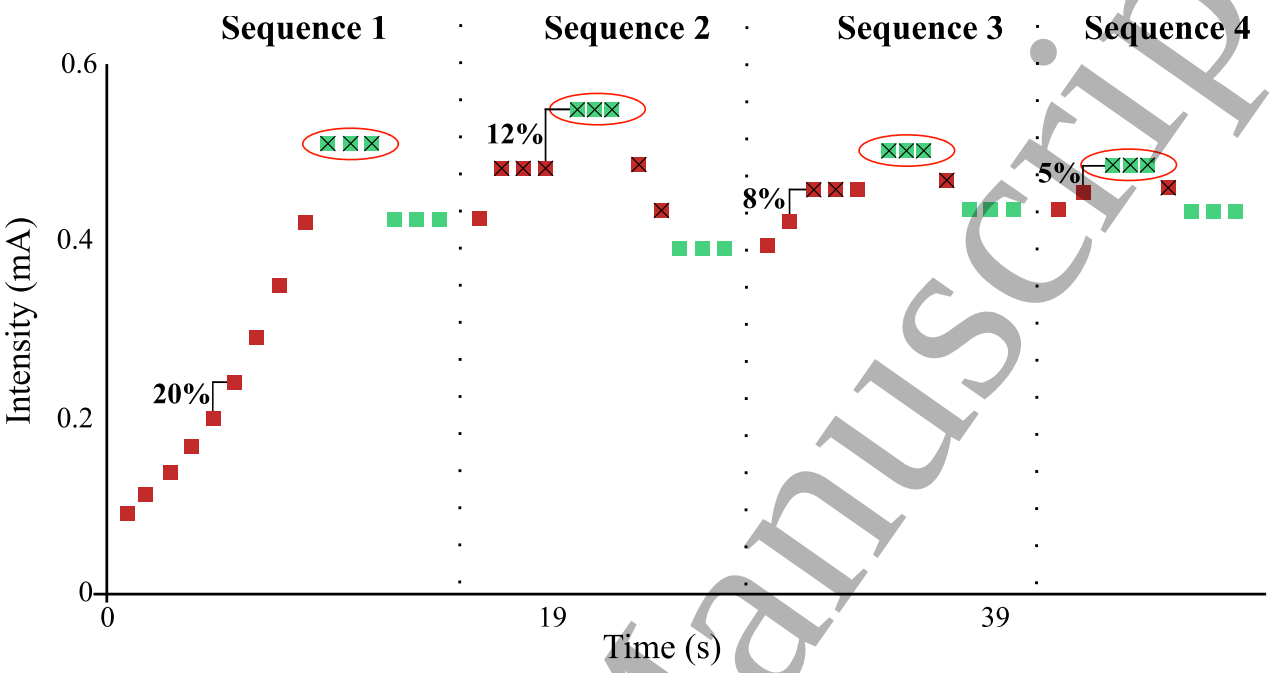

Figure 3: Example of the modified method of limits used for the determination of the perception threshold. A sequence contained one ascending limit and one descending limit. The limits were defined as three consecutive felt or not felt stimuli at the same intensity for ascending and descending limits, respectively. Squares indicate the time and intensity of the stimulation and every square with a cross indicate a perceived stimulus as the subject pressed the button. The green squares indicate the limits used to estimate the perception threshold. The step size for sequence 1, 2, 3, and 4 were 20 %, 12 %, 8 %, and 5 %, respectively. The circled ascending limits indicate the stimuli for which reaction times were analyzed further.

2.4 Statistical Analysis

Statistical analysis on the experimental data was performed using SPSS statistics (Version 24.0. Armonk, NY: IBM Corp). The reaction time, chronaxie, and rheobase measures were non-normally distributed and consequently log-transformed prior to the statistical tests. A linear mixed model analysis was performed for each of the three dependent parameters. The linear mixed model for the chronaxie and rheobase included the main effect of the electrode as a repeated fixed effect and a random intercept for each subject. For reaction times the main effects pulse duration and electrode were included as repeated fixed effects. The duration-electrode interaction was likewise set as a fixed effect. A random intercept for each subject was included and the recording number for each of the 12 included reaction times for each subject, pulse and electrode, were included as a repeated covariate.

Additionally, to account for the difference between the dominant and non-dominant hand, the arm of stimulation was introduced as a covariate. The autoregressive repeated-measures covariance structure was applied, as the data was expected to have homogeneous variance and inhomogeneous covariance, meaning the variability of the measurements is constant, but the covariance between measures that are close in time is larger than measurements far apart. For significant main effects, pairwise comparisons were performed, using Bonferroni correction for multiple comparisons. A p-value of less than 0.05 was considered statistically significant.

3. Results

3.1 The electrical potential produced in the skin

All electrodes, except the regular patch, produced a substantially higher electrical potential in the epidermis than in the dermis and had a large drop in potential throughout the epidermal layer. The intra-epidermal electrode and the planar array electrode additionally exhibited a drop in the electrical potential throughout the dermal layer, which was not as pronounced for the planar array and the pin electrode, see figure 4(A-F). The intra-epidermal electrode produced the highest electrical potential in the epidermis (13.87 V) and additionally expressed the largest drop in potential in both the epidermal and dermal skin layer, see figure 4(A).

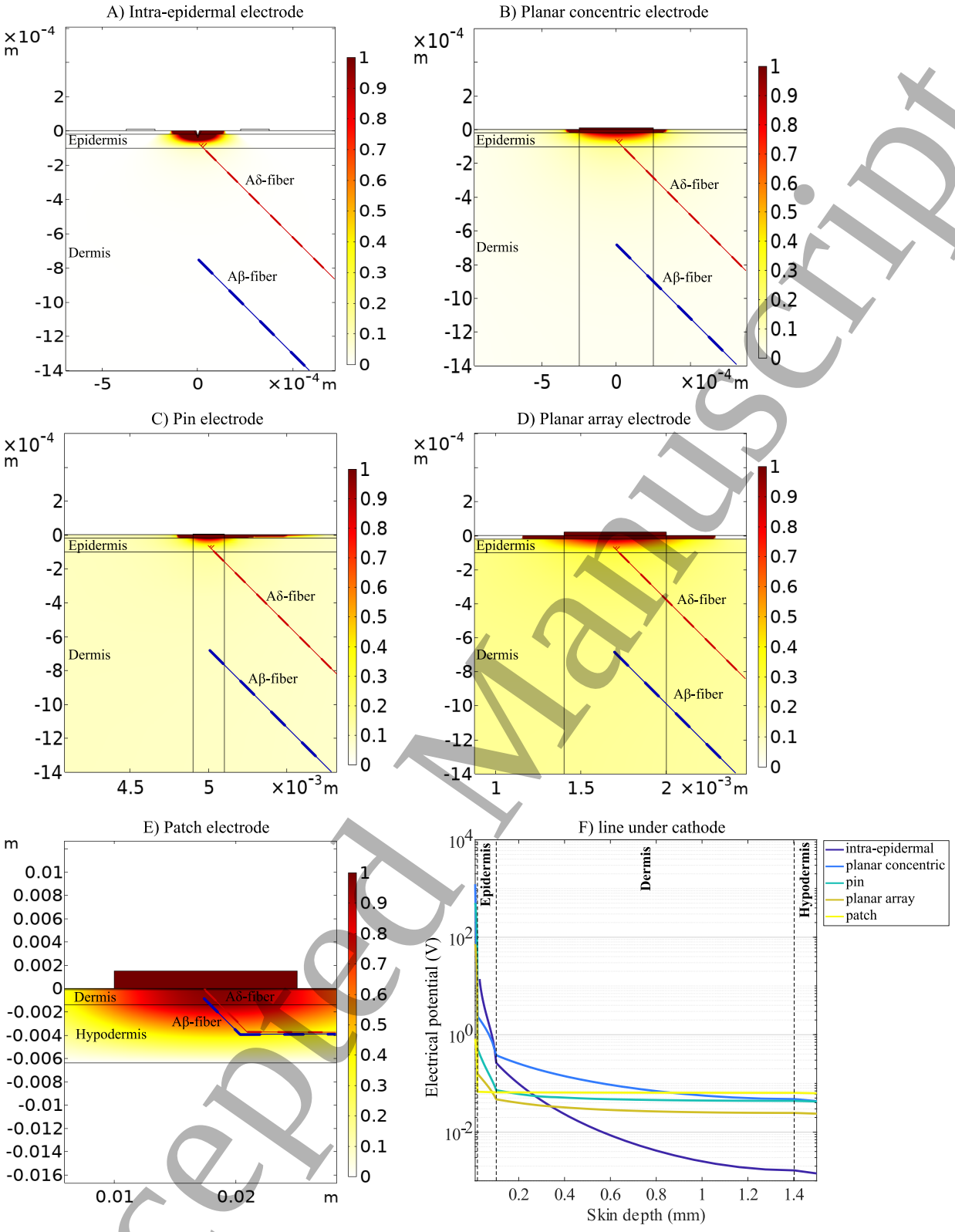

Figure 4: The distribution of the electrical potential within the stratum corneum, epidermis and dermis, for the five electrodes. Electrical potentials (A, B, C, D, E) are normalized to the maximum potential observed in the middle of the epidermal layer. F, shows the drop in the electrical potential through the skin (not normalized), at a straight line under the cathode. The electrical potential underneath the intra-epidermal electrode starts in the epidermis at a skin depth of 30 µm, and not at the stratum corneum, due to the needle penetration.

3.2 Electrode and skin model impedance

To validate the finite element model of the skin and electrode-skin interface, experimental impedances were acquired for frequencies between 10 Hz and 100 kHz (see figure 5). Due to noise, the 50 Hz data were discarded. The electrode-skin interface can be viewed as a parallel capacitance and resistance, in series with the bulk impedance between the anode and cathode, resulting in decreasing impedance with increasing frequency [46] (see figure 5F illustrating the impedance contribution of the inter and skin to the total impedance). At low frequencies mainly, the electrode resistance can be observed as a constant impedance (particularly visible for the pin electrode, figure 5(C)). With increasing frequency, the electrode capacitance becomes more and more dominant in the impedance spectrum (visible for all electrodes, figure 5(A-E). At the highest frequencies, the electrode capacitance is shorted and the bulk impedance, which is considered mainly resistive, becomes visible in the spectrum (best shown for the patch electrode, figure 5(E-F)).

The impedances calculated by the computational model followed the same pattern as the experimentally obtained impedances and were for the most part within one standard deviation of the experimental data. However, the planar concentric electrode model slightly overestimated the impedance, and the planar array model primarily underestimated the bulk impedance. Measured impedances for the patch electrode ranged between 450 Ω, reflecting the bulk skin impedance, and 170 k Ω, reflecting the impedance of the anode and cathode. This was the lowest observed impedance spectrum for all the electrodes. For the pin, planar concentric and planar array electrodes the impedances were similar across the frequency spectrum and in the kΩ- MΩ range. The Pin electrode did however, exhibit lower impedance than the planar concentric and planar array electrodes at the low frequencies. The intra-epidermal electrode had the highest impedances (15k Ω -14MΩ).

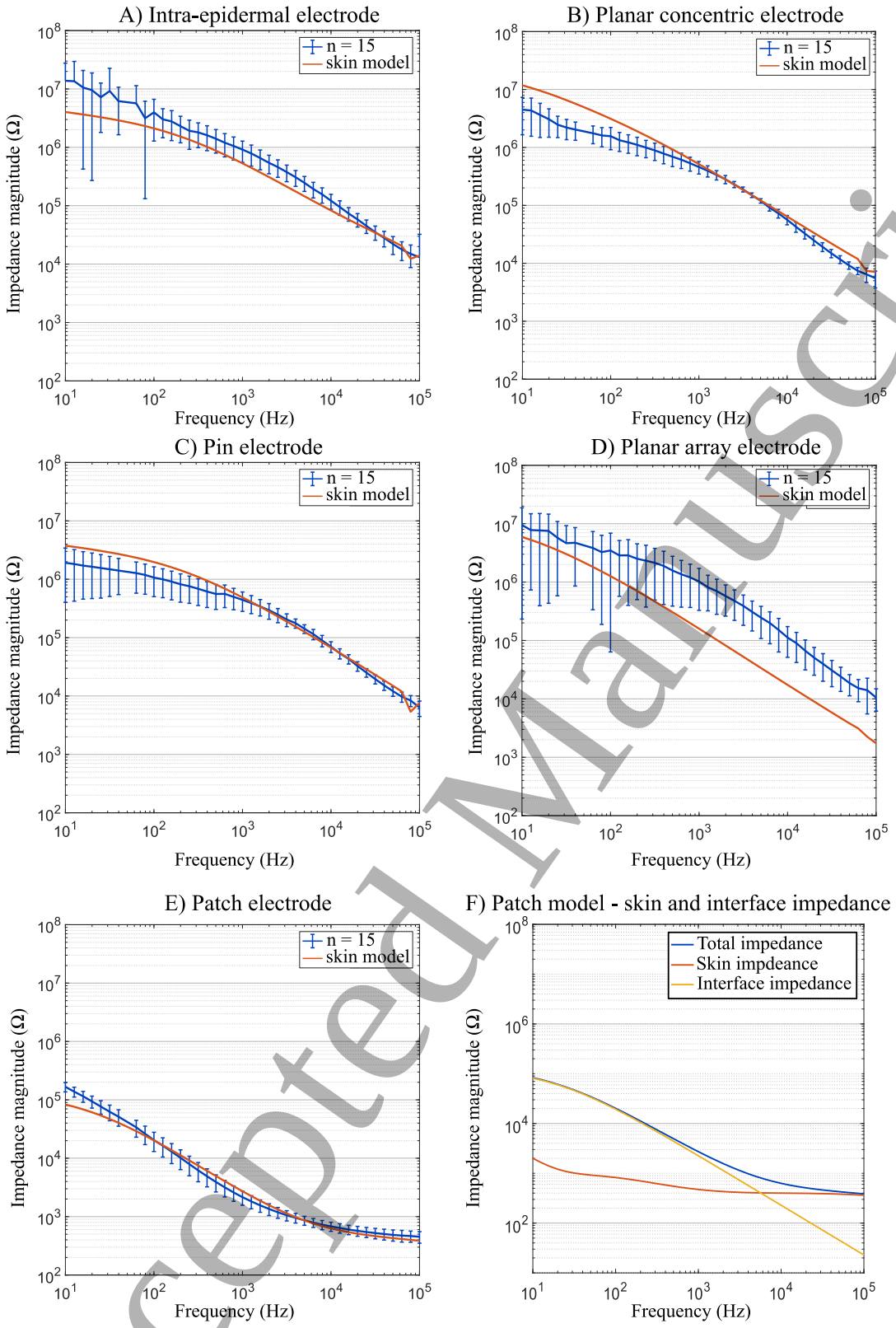

Figure 5: Experimental (mean and standard deviation) and model impedance magnitude of the five different electrodes in the frequency range from 10 Hz to 100 kHz. A) Impedance response of the intra-epidermal electrode. B) Impedance response of the planar concentric electrode. C) Impedance response of the pin electrode. D) Impedance response of the

planar array electrode. E) Impedance response of the patch electrode. F) Modelled impedance response for the patch electrode, illustrating the contributions of the interface impedance and the skin impedance to the total impedance.

3.3 Strength-duration curves

The nerve fiber models were activated at the nerve fiber ending, when stimulation was provided through electrodes preferential for the specific fiber type (Aδ-fiber model: small area electrodes, Aβ-fiber model: patch electrode). The normalized strength-duration curves showed the model predictions to lie within one standard deviation of the experimental data, for most of the pulse durations, for all electrodes (figure 6(A-E)). The model predictions for the regular patch electrode were slightly underestimated, most pronounced for the 0.1 ms pulse duration. Rheobases and chronaxies were estimated by Weiss law and are listed in table 3 (see coefficient of determination values in supplementary table S5). The rheobase values of the electrodes designed for small fiber activation were all significantly smaller than for the regular patch electrode ($p < 0.01$). The chronaxie values for the small fiber electrodes additionally depict a wider interquartile range (IQR) than the patch, however no significant differences in chronaxies were found between any of the electrodes ($p = 0.764$).

Table 3: Median and interquartile range (IQR) for experimental and model estimations of rheobase, and chronaxie for each of the electrodes.

Electrode	Rheobase mA (IQR)	Computational model Rheobase mA (IQR)	Computational model Chronaxie µs (IQR)	Chronaxie µs (IQR)
Intra-epidermal	0.168 (0.111-0.205)	0.1302(0.057-1.037)	654 (210-1,527)	750 (496-1,223)
Planar concentric	0.222 (0.104-0.310)	0.0425 (0.026-0.157)	723 (614-776)	711 (319-1,310)
Pin	0.107 (0.090-0.146)	0.092 (0.088-0.201)	869 (741-976)	599 (416-1,375)
Planar array	0.151 (0.116-0.237)	0.689 (0.373-0.730)	533 (415-645)	756 (434-1,275)
Patch	0.381 (0.334-0.412)	0.210 (0.206-0.217)	461 (432-467)	687 (544-762)

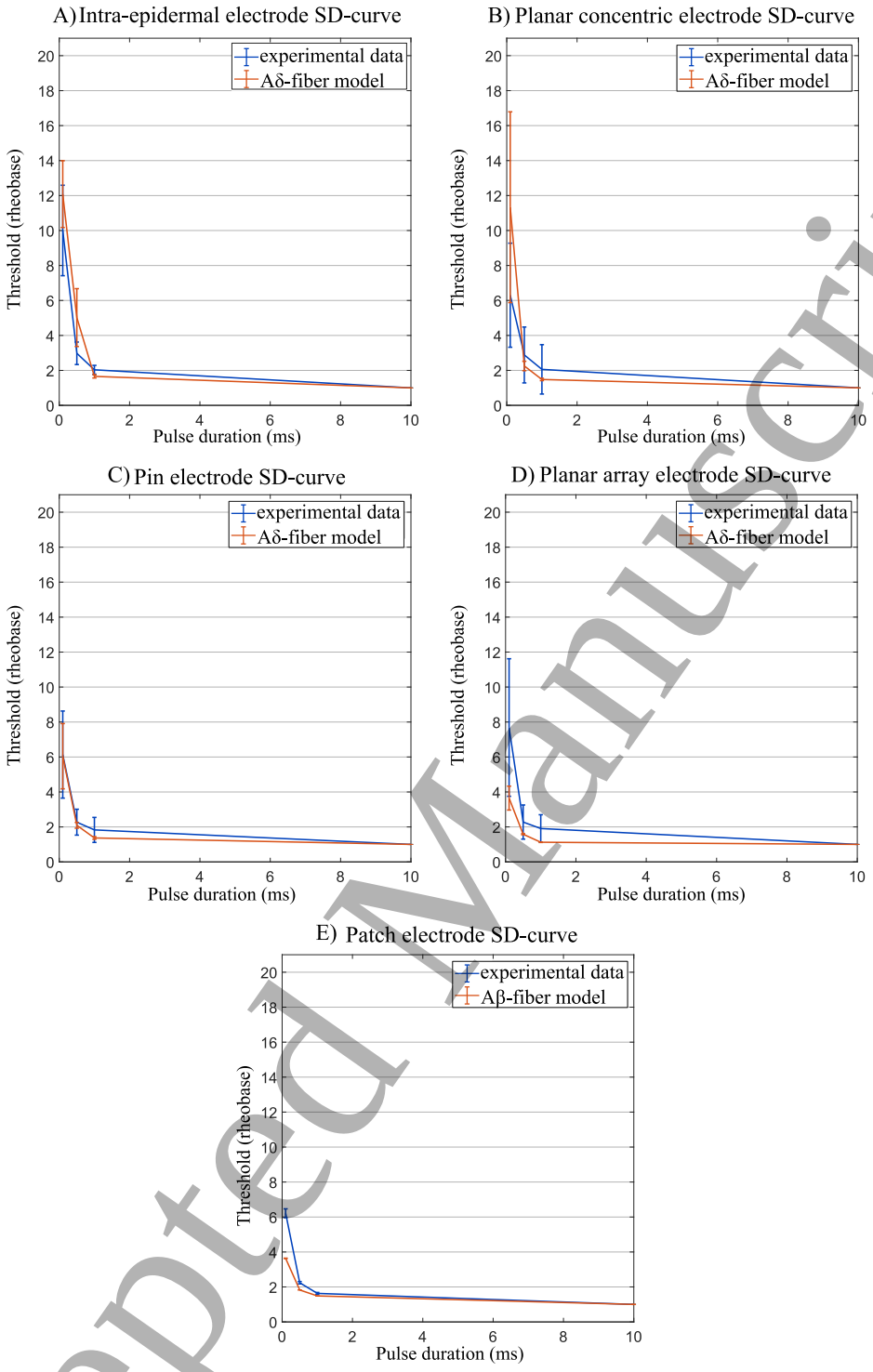

Figure 6: Average of the experimentally obtained and modeled strength-duration curves (SD-curves) normalized to rheobase, for all electrodes. The modelled nerve fiber for each electrode correspond to the nerve fiber model for which the electrode achieved the lowest activation threhsold, and thereby the nerve fiber population that is preferentially activated for the specific electorde. Error bars indicate standard deviations across subjects for the experimental data and standard deviations across nerve fiber locations for the modelling results. A) SD-curve for the intra-epidermal electrode and Aδ-fiber model. B) SD-curve for the planar concentric electrode and Aδ-fiber model. C) SD-curve for the pin electrode and Aδ-fiber model. D) SD-curve for the planar array electrode and Aδ-fiber model. E) SD-curve for the patch electrode and Aβ-fiber model.

3.4 Area of selectivity

The area for which the electrodes are selective for activation of Aδ-fibers is depicted in figure 7. With a 10 ms stimulation pulse the area of selectivity was largest for the planar array (2.69 mm^2) and the pin (1.14 mm^2) electrode, due to the multiple cathode design, where each cathode produced a selective area of activation of 0.22 mm^2 and 0.08 mm^2, for the planar array and pin electrode, respectively. With a 0.1 ms stimulation pulse the planar array was not selective for Aδ-fibers at any location. Additionally, the area of selectivity produced by the planar array electrode was restricted to the superficial part of the epidermis ($z = 21$ μm) and was no longer present in the middle of the epidermal layer ($z = 61$ μm). The pin did produce an area of selectivity in the superficial layer for the 0.1 ms (0.04 mm^2) pulse and the middle of the epidermis for the 10 ms pulse (0.17 mm^2). However, for the 0.1 ms pulse condition the area of selectivity produced by the pin was smaller than the areas produced by the intra-epidermal (0.12-0.13 mm^2) and planar concentric electrode (0.16-0.32 mm^2). For the 10 ms stimulation pulse the intra-epidermal and planar concentric electrode produces areas of Aδ-fiber selectivity of 0.16 mm^2 and 0.64-0.81 mm^2, respectively. None of the electrodes were selective at the deep fiber location in the epidermis ($z = 101$ μm).

The intra-epidermal electrode generated the smallest area of selectivity, however the ratio between the activation thresholds of the nerve fiber models, were highest for this electrode (15-200.7). The maximum ratio for the planar concentric, pin, and planar array electrode were 11.6, 3.44, and 1.42, respectively.

Increasing the pulse duration increased both the activation ratio and the area of selectivity for all electrodes. The largest increase in selective area was observed for the planar array electrode (2.69 mm^2), while the largest increase in ratio was observed for the intra-epidermal electrode (303 %).

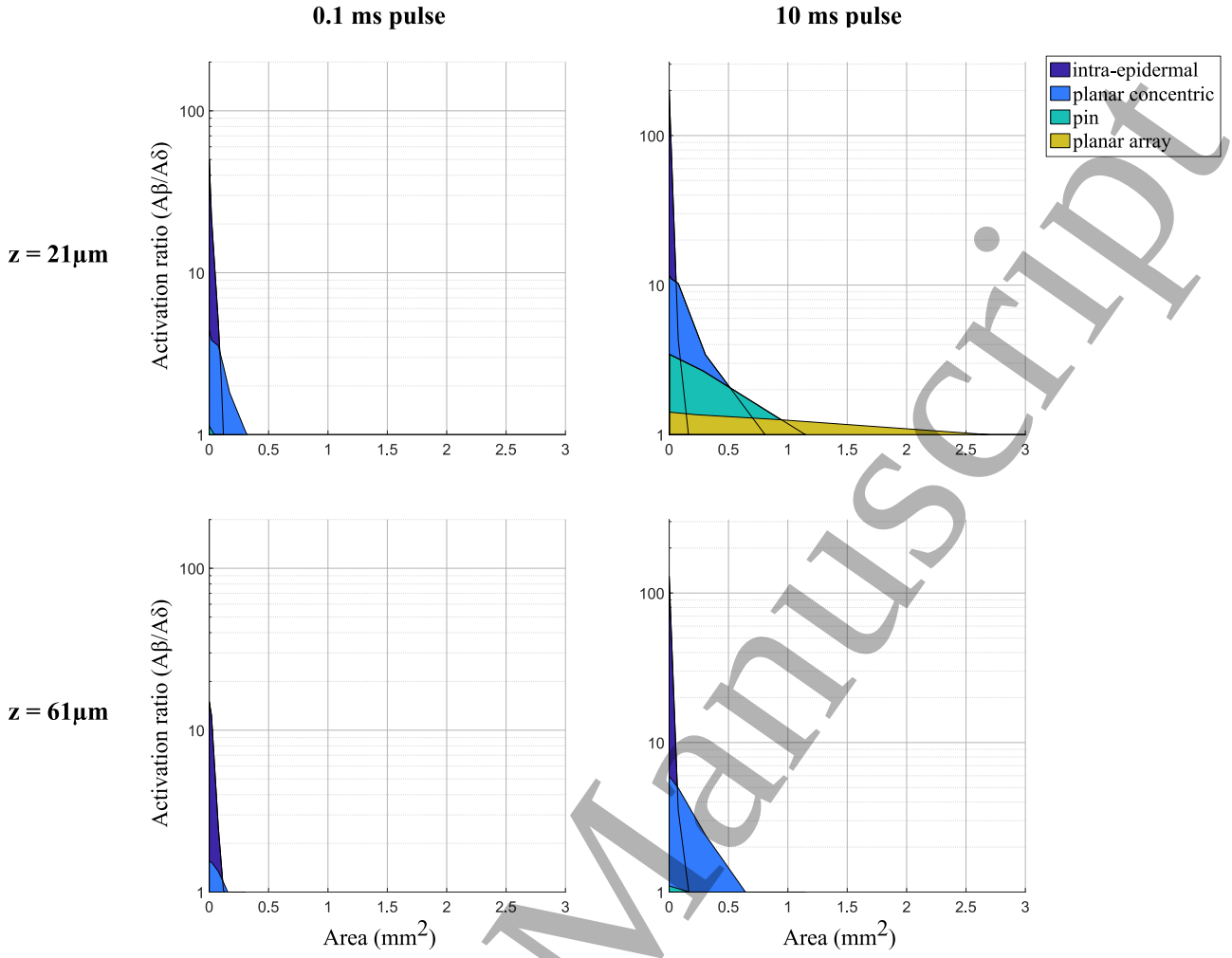

Figure 7: Area of selectivity and current activation threshold ratio between the current activation thresholds of the large Aβ-fiber model and the current activation threshold of the small Aδ-fiber model, for small area electrodes. A ratio above 1 indicates selectivity for Aδ-fibers. Columns represent 0.1 and 10 ms rectangular stimulation pulses, while rows represent the depth (z) of the location of the Aδ-fiber model.

3.5 Reaction time

Reaction times were acquired during the estimation of the perception threshold (see figure 8). All of the electrodes designed for small fiber activation had longer reaction times than the regular patch electrode ($p < 0.001$). The reaction times for intra-epidermal stimulation was significantly longer than for the other electrodes ($p < 0.001$). The planar concentric electrode exhibited significantly longer reaction times than the planar array electrode ($p < 0.001$), but neither the planar concentric nor the planar array electrode had reaction times significantly different from the pin electrode. An effect of pulse duration was found between the shortest 0.1 ms and longest 10 ms pulses, where reaction times for the short pulse on average was 15 ms faster than for the 10 ms pulse. No interaction effect was found between the electrodes and the pulse durations ($p = 0.466$).

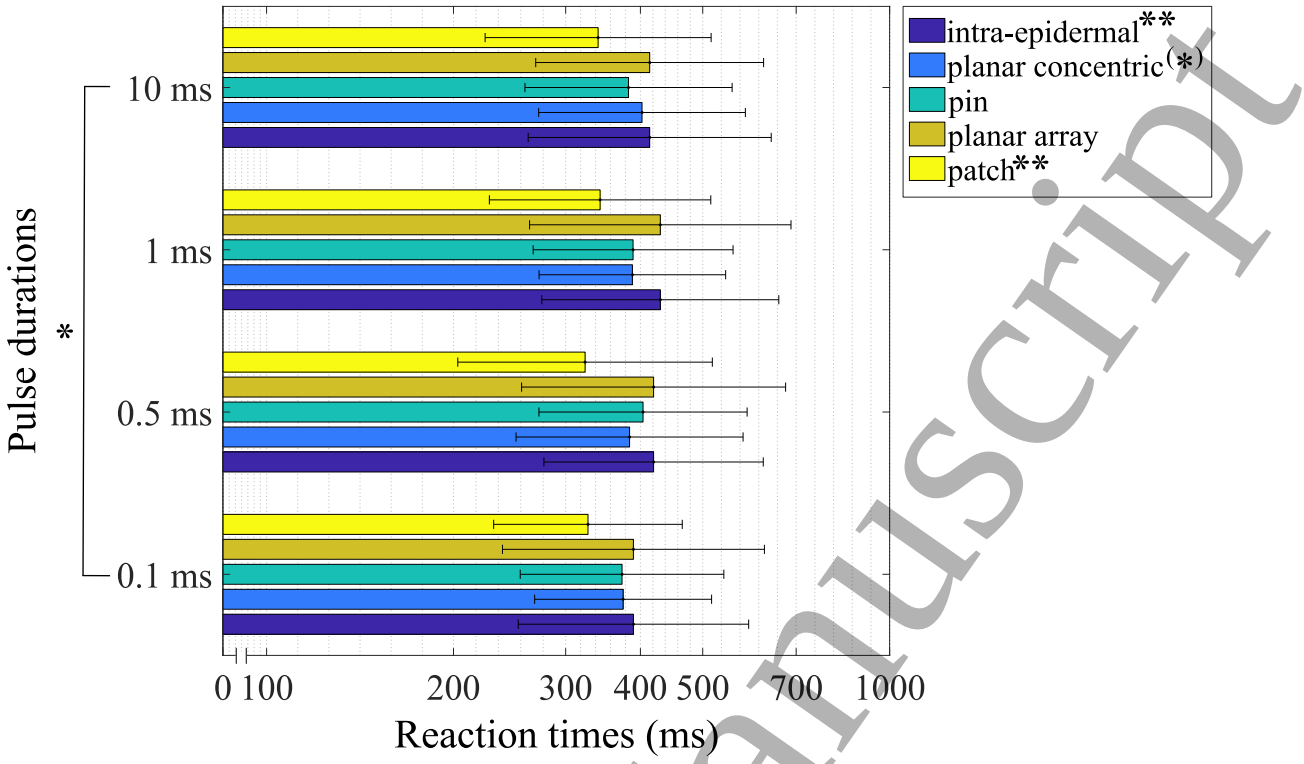

*Figure 8: Average and standard deviation of the log-transformed reaction times, for all electrodes and pulse durations. * Indicates a significant difference between the shortest and longest stimulation pulse. ** Indicates a significant difference between the patch electrode and all the other electrodes, and between the intra-epidermal electrode and all the other electrodes. (*) indicates that significantly longer reaction times were observed for the planar concentric electrode when compared to the planar array electrode.*

4. Discussion

Preferential small fiber activation by electrical stimulation was investigated through the development of a finite element model of the skin and the electrode-skin interface, in combination with nerve fiber models of an Aδ-fiber and an Aβ-fiber. The results of the computational model predicted all electrodes except the regular patch to be preferential for small fibers, however, not to the same degree. The intra-epidermal electrode produced a higher current density in the epidermal layer and less current spread to deeper tissues than the other electrodes. This profile of the electrical potential in the skin led to a higher threshold ratio between large and small fibers for the intra-epidermal electrode, suggesting this electrode type to be the most preferential electrode for small fibers. However, the area of preferential activation in the superficial epidermis was smaller for the intra-epidermal electrode than for the planar concentric and pin electrode.

The computational model was validated through impedance measurements, assessments of perception thresholds, and reaction times.

4.1 Preferential small fiber activation

The intra-epidermal, planar concentric and pin electrodes have previously been found to elicit pinprick like sensations, indicating Aδ-fiber activation [8], [9], [18]. These findings agree with the present computational model that predicts the electrodes to activate small fibers at a lower intensity than large fibers. However, the preferential activation of small fibers has been greatly debated for these electrodes. Katsarava et al [47] found the pinprick sensation and the evoked potentials, elicited by the planar concentric electrode, to be abolished after application of local anesthetics, mainly affecting small fibers. On the contrary, La Cesa et al [16] found that the pinprick sensation was only reduced after capsaicin-induced nerve fiber denervation and the latency of evoked potentials was not altered, indicating that concomitant activation of Aβ-fibers occurs even at low stimulation intensities, slightly over perception threshold. Mouraux et al [7] similarly, found the intra-epidermal electrode to concomitantly activate a substantial degree of Aβ-fibers when the stimulation intensity increased above two times perception threshold. Furthermore, latency findings of evoked potentials elicited by the planar concentric electrode are conflicting as they have been found to both be within the Aδ-fiber range [47], [48] and to be too short for Aδ-fiber activation [14]. The present study suggests that the planar concentric electrode is Aδ-fiber preferential, as the Aδ-fiber model needed less current to

activate than the Aβ-fiber model and as the reaction times were significantly longer for the planar concentric electrode than for the regular patch electrode. However, some Aβ-fibers may lie more superficial in the dermal layer and consequently, a small proportion of Aβ-fibers could be activated at lower intensities, which may account for shorter evoked potential latencies, despite the pinprick sensation. Additionally, it is important to notice that the presented model is a single fiber model, however to achieve perception, single fiber stimulation is not sufficient [49], [50]. Consequently, nerve fibers in the present model are to be considered as principal representations of a larger population of similar nerve fibers.

4.2 Effects of electrode design

Common for all the electrodes for small fiber activation is the small area cathode(s), which has been shown to be important for generating a high current density in the epidermal layer and thus for the preferential activation of small fibers, as these terminate in the epidermis [13]. Of the electrodes investigated in the present study, the intra-epidermal electrode had the smallest contact surface area for the cathode and generated the highest electrical potential in the epidermis as well. It is however important to notice that the smaller the cathode area is, the more sensitive the electrode will be to the relative nerve fiber location and the larger the impedance. Assuming that the smaller the cathode the more preferential the electrode is for small fibers; the pin electrode should have the second-highest ratio between activation thresholds of the two nerve fiber models. However, this was not the case. The planar concentric electrode had a larger cathode area than the pin and planar array electrodes, but still generated a higher electrical potential in the epidermis and produced a higher ratio between activation thresholds for the Aβ-fiber and Aδ-fiber models. This is likely due to the anode-cathode distance, which is shorter for the planar concentric electrode (2.25 mm), than for the pin (6 mm) and the planar array (7 mm) electrodes. A small distance between the cathode and anode limits the current spread to deeper tissues [9], [11] which can explain why the planar concentric electrode is more preferential for small fibers than the pin and planar array. Additionally, the anode area differs between the electrodes, which may be a contributing factor to the difference of the electrical potential produced within the dermis for the pin and planar concentric electrodes. The planar concentric electrode has a steeper decrease of the electrical potential within the dermis than does the pin electrode, limiting the amount of current reaching the Aβ-fiber model. This could explain the larger activation ratio for the nerve fiber models observed for the planar concentric electrode compared to the pin electrode. The

limited current spread to deeper tissues may also be the basis for the larger selective area produced in the middle of the epidermis by the planar concentric electrode compared to the pin electrode.

The intra-epidermal electrode was the only investigated electrode with a needle shape. This shape has been shown to be able to target nerve fibers at the needle depth and a few micrometers deeper, however, it is crucial that the electrode is long and sufficiently sharp to just penetrate the resistive stratum corneum [20]. Penetrating the stratum corneum will decrease the impedance and provide the possibility to have a very small cathode area and as mentioned produce a higher electrical potential in the superficial epidermis. It is however difficult to know exactly how much the needle penetrates, and penetration depth will vary, as the thickness of the stratum corneum varies both between body regions and between subjects [33], [35]. The stratum corneum dominates the skin impedance in the low frequency range until frequencies of about 1 kHz [51], and the influence of the stratum corneum on the net electrode impedance depends on the needle depth, as the depth determines the contact area of the electrode. The difference in experimentally assessed impedance and model predictions for the intra-epidermal electrode may thus be due to the actual ability of the needle to reach viable tissue. If the needle, experimentally, did not reach 10 μm down the epidermis, the stratum corneum would contribute more to the net impedance and in particular, at lower frequencies the impedance would become higher.

4.3 Area of preferential small fiber activation

In the present study, the needle shape and resulting small cathode-skin contact of the intra-epidermal electrode, limited the area of preferential activation compared to the other electrodes, but made it possible to target small fibers in both the superficial and middle part of the epidermis. This is in agreement with the findings of Motogi et al [20], who additionally showed that the stimulation volume would become deeper and narrower with an increased penetration depth of the electrode. The narrow area of activation makes the electrode sensitive to actual nerve fiber location and limits the reproducibility and the practical use of the electrode, which corresponds to the practical experience with having to be moved the electrode around to achieve a reasonable perception threshold. There seems to be a tradeoff between the area of activation and the effective ratio between large and small fiber activation thresholds. The intra-epidermal electrode has a high ratio, but a small area of

activation, while the planar array electrode has a large activation area, but a low ratio between activation threshold of the large and small fiber models which limits the range of stimulation intensities that can be used for preferential small fiber stimulation.

4.4 Increased preferential activation of small fibers by stimulation pulse

Another approach to increasing the ratio between the activation thresholds of large and small fibers could be to increase the stimulus duration. The computational model predicted the nerve fiber activation ratio to increase with increasing pulse length, which is in agreement with the results of Hugosdottir et al [52] and Jonas et al [53], who showed that long duration current stimulation was able to increase the perception threshold ratio of the patch and pin electrodes. The ratio did not only increase for longer stimuli, but also for pulse shapes with a slow rise time [52]. This approach takes advantage of the differences in voltage gated ion channel distribution between nerve fiber types [21], and the phenomenon of accommodation for large fibers. Accommodation is defined as an increase in activation threshold for a maintained local potential and can be achieved through a slow depolarization of the membrane which leads to sodium channel inactivation [42], [54]. It may thus be important to combine the electrode design with special stimulation currents to maximize preferential activation of small fibers.

4.5 Experimental validation

The model implemented electrical properties for the skin and electrode-skin interface were able to predict the measured electrode impedances within one standard deviation for most of the electrodes. For the planar array electrode the model impedance of the high frequencies were underestimated compared to the experimentally obtained impedances. The contact area for the planar array electrode was higher than the planar concentric electrode due to the multiple cathode design and was thus expected to have a lower impedance than the planar concentric electrode. The high impedance for the planar array electrode may be due to difficulties in achieving good contact between the skin and the electrode, and perhaps not all cathodes have been in contact with the skin making the total cathode

area smaller and thus increasing the impedance. This could additionally explain the model underestimation of impedance for the planar array electrode. The computational model predicted all other electrodes than the regular patch to be able to activate small fibers at lower intensities than large fibers. Additionally, the experimentally measured reaction times indicate that the electrodes designed for small fiber activation activate slower conducting Aδ-fibers to a greater extent than the patch electrode, which is known to preferentially activate Aβ-fibers. The interquartile range of assessed reaction times for the small cathode electrodes was 317-476 ms which is within the range of Aδ-fibers (300-650 ms [19]), while the reaction times interquartile range for the patch electrode was 271-404 ms, which in fact is containing longer reaction times than expected for the Aβ-fibers (< 300 ms). Reaction times are influenced by a lot of different processes and depend on the nerve fiber conduction velocities as well as the attention to the stimuli and the decision processing and the motor execution [55]. These are all factors that cannot not be neglected are not easily controlled, why especially cognitive aspects may have had an influence on the recorded reaction times. We did however try to minimize the attention factor by randomizing the order of the electrodes to even out possible attention drop throughout the experiment and we likewise included several breaks enabling the subjects to keep focus on the stimuli throughout the experiment. Reaction times additionally, become faster with increased stimulation intensity [56], likely due to a faster decision processing of the signal. This may explain the relatively long reaction times as the stimulation intensities used were low, around the perception threshold. Additionally, the rheobase was lower for the electrodes designed for small fiber activation compared to the regular patch. However, the chronaxie values were not significantly different between electrodes, which would mean the strength-duration curve is only shifted vertically and the targeted fiber types did not have different excitability. The difference in rheobase may be explained by the difference in electrode impedance and thereby the cathode area. This would however contradict previous findings by Hennings et al [43] and Hoberg et al [44] who showed the pin and patch electrodes to exhibit differences in both chronaxie and rheobase. The reason that no significant difference was found in the present study may be due to the patch configuration used. The anode in the patch setting was smaller and positioned closer to the cathode than in the previous studies, which may have decreased the current spread in the skin to an extent where a more mixed population of nerve fibers have been activated and resulted in a shift of the strength-duration curve towards less excitability. This may likewise explain the long reaction times seen for the patch electrode.

4.6 Model limitations

The skin was considered homogeneous in order to simplify the model, but in fact the skin is a highly heterogeneous structure and skin appendages such as sweat ducts can have a large influence on the current spread as they are highly conductive [57]. Current flowing through a sweat duct would result in a decreased perception threshold and a current spread to deeper tissues, increasing the possibility of activating large fibers. The nerve fiber models were activated at the tip or at the first node of ranvier for all electrodes, which is likely the reason why, the models were able to predict experimental outcomes despite the mentioned model simplifications.

5. Conclusion

A skin and nerve fiber model was implemented for comparing surface electrodes. The model predicted the intra-epidermal electrode to be the most preferential for activating small nociceptive fibers, which is likely due to the needle shape and the short cathode-anode distance. Even though the needle shape was beneficial for achieving a large ratio between activation thresholds for large and small fibers it was highly sensitive to nerve fiber location as the produced area of small fiber selectivity was limited. Consequently, the electrode may have to be moved around to find a reasonable threshold, which introduces an observer subjectivity to the measurements, why it would be recommended to use either more than one intra-epidermal electrode or use multiple cathodes electrodes. The developed model may be used for electrode optimization to achieve both substantial preferential activation of small fibers and high usability.

Acknowledgments

The authors have no conflict of interest to declare. The presented work has been funded by Center for Neuroplasticity and Pain (CNAP), supported by the Danish National Research Foundation (DNRF121).

References

[1] Lacomis, D., 2002, Small-fiber neuropathy, *Muscle and Nerve*, **26**, 173–188.

[2] Otsuru, N., Inui, K., Yamashiro, K., Miyazaki, T., Takeshima, Y., and Kakigi, R., 2010, Assessing Aδ Fiber Function With Lidocaine Using Intraepidermal Electrical Stimulation, *J. Pain*, **11**, 621–627.

[3] Klein, T., Margerl, W., Hopf, H.-C., Sandkühler, J., and Treede, R.-D., 2004, Perceptual Correlates of Nociceptive Long-Term Potentiation and Long-Term Depression in Humans, *J. Neurosci.*, **24**, 964–971.

[4] Jung, K., Rottmann, S., and Ellrich, J., 2009, Long-term depression of spinal nociception and pain in man: Influence of varying stimulation parameters, *Eur. J. Pain*, **13**, 161–170.

[5] Nilsson, H. J. and Schouenborg, J., 1999, Differential inhibitory effect on human nociceptive skin senses induced by local stimulation of thin cutaneous fibers, *Pain*, **80**, 103–112.

[6] Plaghki, L. and Mouraux, A., 2003, How do we selectively activate skin nociceptors with a high power infrared laser? Physiology and biophysics of laser stimulation, *Neurophysiol. Clin.*, **33**, 269–277.

[7] Mouraux, A., Iannetti, G. D., and Plaghki, L., 2010, Low intensity intra-epidermal electrical stimulation can activate Aδ-nociceptors selectively, *Pain*, **150**, 199–207.

[8] Inui, K., Tran, T. D., Hoshiyama, M., and Kakigi, R., 2002, Preferential stimulation of Aδ fibers by intra-epidermal needle electrode in humans, *Pain*, **96**, 247–252.

[9] Kaube, H., Katsarava, Z., Käufer, T., Diener, H.-C., and Ellrich, J., 2000, A new method to increase nociception specificity of the human blink reflex, *Clin. Neurophysiol.*, **111**, 413–416.

[10] Steenbergen, P., Buitenweg, J. R., Trojan, J., van der Heide, E. M., van den Heuvel, T., Flor, H., and Veltink, P. H., 2012, A system for inducing concurrent tactile and nociceptive sensations at the same site using electrocutaneous stimulation., *Behav. Res. Methods*, **44**, 924–33.

[11] Leandri, M., Marinelli, L., Siri, A., and Pellegrino, L., 2018, Micropatterned surface electrode for massive selective stimulation of intraepidermal nociceptive fibres, *J. Neurosci. Methods*, **293**, 17–26.

[12] Inui, K. and Kakigi, R., 2012, Pain perception in humans: use of intraepidermal electrical stimulation, *J. Neurol. Neurosurg. Psychiatry*, **83**, 551–556.

[13] Mørch, C. D., Hennings, K., and Andersen, O. K., 2011, Estimating nerve excitation thresholds to cutaneous electrical stimulation by finite element modeling combined with a stochastic branching nerve fiber model, *Med. Biol. Eng. Comput.*, **49**, 385–395.

[14] Perchet, C., Frot, M., Charmarty, A., Flores, C., Mazza, S., Magnin, M., and Garcia-Larrea, L., 2012, Do we activate specifically somatosensory thin fibres with the concentric planar electrode? A scalp and intracranial EEG study, *Pain*, **153**, 1244–1252.

[15] de Tommaso, M., Santostasi, R., Devitofrancesco, V., Franco, G., Vecchio, E., Delussi, M., Livrea, P., and Katzarava, Z., 2011, A comparative study of cortical responses evoked by transcutaneous electrical vs CO2 laser stimulation, *Clin. Neurophysiol.*, **122**, 2482–2487.

[16] La Cesa, S. *et al.*, 2018, Skin denervation does not alter cortical potentials to surface concentric electrode stimulation: A comparison with laser evoked potentials and contact heat evoked potentials, *Eur. J. Pain (United Kingdom)*, **22**, 161–169.

[17] Mouraux, A., Iannetti, G., and Plaghki, L., 2010, Selective Activation of Aδ Nociceptors By Low-Intensity Intra-Epidermal Electrical Stimulation, *Eur. J. Pain Suppl.*, **4**, 68–68.

[18] Lelic, D., Mørch, C. D., Hennings, K., Andersen, O. K., and M. Drewes, A., 2012, Differences in perception and brain activation following stimulation by large versus small area cutaneous surface electrodes, *Eur. J. Pain (United Kingdom)*, **16**, 827–837.

[19] Mouraux, A., Marot, E., and Legrain, V., 2014, Short trains of intra-epidermal electrical stimulation to elicit reliable behavioral and electrophysiological responses to the selective activation of nociceptors in humans, *Neurosci. Lett.*, **561**, 69–73.

[20] Motogi, J., Sugiyama, Y., Laakso, I., Hirata, A., Inui, K., Tamura, M., and Muragaki, Y., 2016, Why intra-epidermal electrical stimulation achieves stimulation of small fibres selectively: a simulation study, *Phys. Med. Biol.*, **61**, 4479–4490.

[21] Tigerholm, J., Poulsen, A. H., Andersen, O. K., and Mørch, C. D., 2019, From Perception Threshold to Ion Channels—A Computational Study, *Biophys. J.*, **117**.

[22] Hines, M. L. and Carnevale, N. T., 1997, The NEURON Simulation Environment, *Neural Comput.*, **9**, 1179–1209.

[23] Biurrun Manresa, J. A., Mørch, C. D., and Andersen, O. K., 2010, Long-term facilitation of nociceptive withdrawal reflexes following low-frequency conditioning electrical stimulation: A new model for central sensitization in humans, *Eur. J. Pain*, **14**, 822–831.

[24] Hugosdottir, R., Mørch, C. D., Jørgensen, C. K., Nielsen, C. W., Olsen, M. V., Pedersen, M. J., and Tigerholm, J., 2019, Altered excitability of small cutaneous nerve fibers during cooling assessed with the perception threshold tracking technique, *BMC Neurosci.*, **20**, 1–13.

[25] Yamamoto, T. and Yamamoto, Y., 1976, Electrical properties of the epidermal stratum corneum, *Med. Biol. Eng.*, **14**, 151–158.

[26] Tavernier, A., Dierickx, M., and Hinsenkamp, M., 1993, Tensors of dielectric permittivity and conductivity of in vitro human derms and epiderms., *Bioelectroch.Bioener.*, **30**, 65–72.

[27] Chi, Y. M., Jung, T. P., and Cauwenberghs, G., 2010, Dry-contact and noncontact biopotential electrodes: Methodological review, *IEEE Rev. Biomed. Eng.*, **3**, 106–119.

[28] Pelot, N. A., Thio, B. J., and Grill, W. M., 2018, Modeling Current Sources for Neural Stimulation in COMSOL, *Front. Comput. Neurosci.*, **12**, 1–14.

[29] Yamamoto, T. and Yamamoto, Y., Non-linear electrical properties of skin in the low frequency range, *Medical and Biological Engineering and Computing*, **19**. 302–310, 1981.

[30] Böhling, A., Bielfeldt, S., Himmelmann, A., Keskin, M., and Wilhelm, K. P., 2014, Comparison of the stratum corneum thickness measured in vivo with confocal Raman spectroscopy and confocal reflectance microscopy, *Ski. Res. Technol.*, **20**, 50–57.

[31] Rajadhyaksha, M., González, S., Zavislan, J. M., Anderson, R. R., and Webb, R. H., 1999, In vivo confocal scanning laser microscopy of human skin II: Advances in instrumentation and comparison with histology, *J. Invest. Dermatol.*, **113**, 293–303.

[32] Huzaira, M., Rius, F., Rajadhyaksha, M., Anderson, R. R., and González, S., 2001, Topographic variations in normal skin, as viewed by in vivo reflectance confocal microscopy, *J. Invest. Dermatol.*, **116**, 846–852.

[33] Sandby-Møller, J., Poulsen, T., and Wulf, H. C., 2003, Epidermal Thickness at Different Body Sites: Relationship to Age, Gender, Pigmentation, Blood Content, Skin Type and Smoking Habits, *Acta Derm. Venereol.*, **83**, 410–413.

[34] Neerken, S., Lucassen, G. W., Bisschop, M. a., Lenderink, E., and Nuijs, T. (a. M. ., 2004,

Characterization of age-related effects in human skin: A comparative study that applies confocal laser scanning microscopy and optical coherence tomography, *J. Biomed. Opt.*, **9**, 274.

[35] Egawa, M., Hirao, T., and Takahashi, M., 2007, In vivo estimation of stratum corneum thickness from water concentration profiles obtained with raman spectroscopy, *Acta Derm. Venereol.*, **87**, 4–8.

[36] Krackowizer, P. and Brenner, E., 2008, Dicke der Epidermis und Dermis* sonographische Messung an 24 Stellen des Menschlichen Körpers, *Phlebologie*, **37**, 83–92.

[37] Gabriel, C., Gabriel, S., and Corthout, E., 1996, The dielectric properties of biological tissues: I. Literature survey, *Phys. Med. Biol.*, **41**, 2231–2249.

[38] Gabriel, S., Gabriel, C., and W, L. R., 1996, The dielectric properties of biological tissues: II. Measurements in the frequency range 10 Hz to 20 GHz, *Phys. Med. Biol.*, **41**, 2251–2260.

[39] Ebenezer, G. J., Hauer, P., Gibbons, C., McArthur, J. C., and Polydefkis, M., 2007, Assessment of epidermal nerve fibers: a new diagnostic and predictive tool for peripheral neuropathies., *J. Neuropathol. Exp. Neurol.*, **66**, 1059–1073.

[40] McArthur, J. C., Stocks, E. A., Hauer, P., Cornblath, D. R., and Griffin, J. W., 1998, Epidermal Nerve Fiber Density, *Arch. Neurol.*, **55**, 1513.

[41] Geddes, L. A. and Bourland, J. D., 1985, The Strength-Duration Curve, *IEEE Trans. Biomed. Eng.*, **32**, 458–459.

[42] Hill, A. V., 1935, Excitation and Accomodation in Nerves, *Proceesings R. Soc. London, Biol. Sci.*, 305–355.

[43] Hennings, K., Frahm, K. S., Petrini, L., Andersen, O. K., Arendt-Nielsen, L., and Mørch, C. D., 2017, Membrane properties in small cutaneous nerve fibers in humans, *Muscle Nerve*, **55**, 195–201.

[44] Hoberg, T. N., Frahm, S., Hennings, K., Arendt-Nielsen, L., and Mørch, C. D., 2019, Assessing the modulation of cutaneous sensory fiber excitability using a fast perception threshold tracking technique, *Muscle Nerve*, 1–8.

[45] Mogyoros, I., Kiernan, M. C., and Burke, D., 1996, Strength-duration properties of human peripheral nerve., *Brain*, **119**, 439–447.

[46] McAdams, E. T., Jossinet, J., Lackermeier, A., and Risacher, F., 1996, Factors affecting electrode-gel-skin interface impedance in electrical impedance tomography, *Med. Biol. Eng. Comput.*, **34**, 397–408.

[47] Katsarava, Z., Ayzenberg, I., Sack, F., Limmroth, V., Diener, H. C., and Kaube, H., 2006, A novel method of eliciting pain-related potentials by transcutaneous electrical stimulation, *Headache*, **46**, 1511–1517.

[48] Lefaucheur, J. P., Ahdab, R., Ayache, S. S., Lefaucheur-Ménard, I., Rouie, D., Tebbal, D., Neves, D. O., and Ciampi de Andrade, D., 2012, Pain-related evoked potentials: A comparative study between electrical stimulation using a concentric planar electrode and laser stimulation using a CO 2 laser, *Neurophysiol. Clin.*, **42**, 199–206.

[49] Johansson, R. S. and Vallbo, A. B., 1979, Detection of tactile stimuli. Thresholds of afferent units related to psychophysical thresholds in the human hand., *J. Physiol.*, **297**, 405–422.

[50] Ochoa, J. and ToreBjörk, E., 1989, Sensation evoked bt intraneural microstimulation of c nociceptor fibers in human skin nerves, *J. Physiol.*, **415**, 583–599.

[51] Birgersson, U. H., Birgersson, E., and Ollmar, S., 2012, Estimating electrical properties and the thickness of skin with electrical impedance spectroscopy: Mathematical analysis and measurements,

J. Electr. Bioimpedance, **3**, 51–60.

[52] Hugosdottir, R., Mørch, C. D., Andersen, O. K., Helgason, T., and Arendt-Nielsen, L., 2019, Preferential activation of small cutaneous fibers through small pin electrode also depends on the shape of a long duration electrical current, *BMC Neurosci.*, **20**.

[53] Jonas, R. *et al.*, 2018, Tuning in C-Nociceptors to Reveal Mechanisms in Chronic Neuropathic Pain, 945–957.

[54] Baker, M. and Bostock, H., 1989, Depolarization Changes the Mechanism of accommodation in rat and human motor axons, *J. Physiol.*, **411**, 545–561.

[55] Campbell, J. N. and Lamotte, R. H., 1983, Latency to Detection of First Pain, **266**, 203–208.

[56] Lakhani, B., Vette, A. H., Mansfield, A., Miyasike-daSilva, V., and McIlroy, W. E., 2012, Electrophysiological Correlates of Changes in Reaction Time Based on Stimulus Intensity, *PLoS One*, **7**.

[57] Sha, N., Kenney, L. P. J., Heller, B. W., Barker, A. T., Howard, D., and Moatamedi, M., 2008, A finite element model to identify electrode influence on current distribution in the skin, *Artif. Organs*, **32**, 639–643.

"The authors have confirmed that any identifiable participants in this study have given their consent for publication".